

PAPER • OPEN ACCESS

Simulating hybrid protection against ultrashort pulse based on its modal decomposition

To cite this article: A V Nosov *et al* 2019 *J. Phys.: Conf. Ser.* **1353** 012022

View the [article online](#) for updates and enhancements.



IOP | ebooks™

Bringing you innovative digital publishing with leading voices to create your essential collection of books in STEM research.

Start exploring the collection - download the first chapter of every title for free.

Simulating hybrid protection against ultrashort pulse based on its modal decomposition

A V Nosov, A O Belousov, R S Surovtsev and T R Gazizov

Tomsk State University of Control Systems and Radioelectronics, 40, Lenin Ave., Tomsk, 634050, Russia

E-mail: alexns2094@gmail.com

Abstract. The paper considers the possibility of hybrid protection against an ultrashort pulse which is based on cascade connection of a modal filter and a turn of a meander line. A qualitative analysis of ultrashort pulse decomposition into 9 pulses of smaller amplitude in this hybrid device is performed and the conditions for such decomposition are formulated. The quasistatic simulation of the time response showed 9.8 times attenuation of the ultrashort pulse.

1. Introduction

A steady increase and development of electronic equipment (EE) and its penetration in almost all spheres of human activity force developers to pay particular attention to ensuring electromagnetic compatibility (EMC). Thus, there is a decrease of EE operating voltages, increase of its operating frequencies and packaging density of printed circuit boards (PCB) in EE, which lead to an increase of EE susceptibility to various electromagnetic interferences (EMI). In addition, the annual growth of the number of EE and the degree of its integration increases the risk of its damage from pulsed [1] and continuous [2] interference, even with a small field strength amplitude. One of the EMC tasks is to protect EE against conductive effects, which are EMI that penetrates the equipment directly through conductors [3]. A dangerous EMI is a high power ultrashort pulse, which can penetrate into EE due to its wide spectrum and disable it due to the high power [4, 5]. To protect EE against EMI, various circuitry and constructive solutions are used, for example, voltage limiters, varistors, passive RC and LC filters, which have a number of disadvantages, the main of which are low power and operation speed, as well as low radiation resistance and, as a result, low operational life [3]. In this regard, traditional means often cannot provide consistent protection for EE against ultrashort pulses [6], therefore, it is necessary to search for and do research into the new ways of effective protection.

There has been plenty of research into various strip-line devices to provide protection against ultrashort pulses and signal filtering in the frequency domain [7–12]. To protect against ultrashort pulses, the authors have proposed modal filters (MF) based on modal decomposition technology, which are devoid of the above mentioned drawbacks and, in addition, have several advantages (no semiconductor components, long operational life, operation at high voltages and low cost). A number of studies have been performed into the use of multiconductor MFs. For example, the researchers [13] present a systematic study of multiconductor MFs in which they have performed analysis of such MFs, considered the possibility of optimization by various criteria, and built a hybrid optimization, which included a heuristic search and a genetic algorithm. In addition, they have performed experimental confirmation of modal filtration based on multiconductor microstrip lines. For example, for 2- and 3-conductor



microstrip lines, attenuation of 11.5 and 13.7 times was obtained. Another method based on signal decomposition into modes is the approach to protecting against ultrashort pulses based on its decomposition in the turn of a meander microstrip line into a sequence of pulses of lower amplitude [14]. The choice of line parameters provides several simple conditions due to which the ultrashort pulse is decomposed into three main pulses with smaller amplitude relative to the initial one. The first pulse is crosstalk at the near end of the line, which comes to the end of the turn at the moment when the main signal appears in the line. The second and third pulses (for simplicity, we will call them the pulses of the even and odd modes of the signal) are the result of the even and odd signal modes separation in time. There is a noteworthy study of the ultrashort pulse decomposition into a sequence of 9 main pulses in the meander microstrip line, which consists of two cascaded turns [14], in which new conditions are obtained, which allow for such decomposition and increased attenuation of the ultrashort pulse.

Despite multiple studies into the MF and meander microstrip lines, their combined use to attenuate an ultrashort pulse has never been explored. Meanwhile, the cascade connection of the MF and the meander microstrip line can increase the attenuation of the ultrashort pulse (due to decomposition of each pulse from the MF output in the meander line), with a relatively small increase in the mass and size parameters of the final device (in contrast to the cascade connection of several MFs). Therefore, such study is relevant. In this case, it is advisable to use a 3-conductor MF, since the number of main decomposed pulses at its output is comparable to one turn of a meander line. It is similar to the study of the meander line of two turns [16], in which the input of the second turn sees the arrival of three pulses which are the result of ultrashort pulse decomposition in the first turn. Then the analysis of the cascaded 3-conductor MF and the meander microstrip line will be similar to the analysis of the meander microstrip line of two turns.

Thus, the aim of this paper is to investigate the possibility of ultrashort pulse decomposition in a cascade of a 3-conductor MF and a turn of a meander microstrip line. To achieve this aim it is necessary: to carry out a preliminary analysis of the ultrashort pulse decomposition and to determine the number of the main decomposed pulses at the end of the device; to formulate the conditions that allow ultrashort pulse decomposition at the end of the device; to perform the device simulation with the parameters satisfying the formulated conditions; to perform the analysis of the obtained results.

2. Structure and diagram for simulation

Figure 1 shows cross-sections of a 3-conductor MF (a) and a meander microstrip line, respectively (b), where, for the MF and the meander line, w_{MF} and w_{ML} are conductor widths; t_{MF} and t_{ML} are conductor thicknesses; s_{1MF} , s_{2MF} and s_{ML} are spaces between conductors; h_{MF} and h_{ML} are the PCB substrate thicknesses; ϵ_{rMF} and ϵ_{rML} are the dielectric permittivity of the substrate.

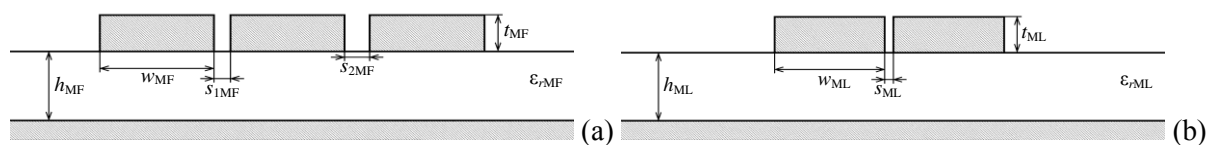


Figure 1. Cross-section of a 3-conductor MF (a) and a meander microstrip line turn (b)

Figure 2 shows the circuit diagram of the device under investigation. It is a 3-conductor MF connected in cascade with a meander microstrip line. The 3-conductor MF consists of three parallel conductors with a length l_{MF} , one of the conductors is connected at one end with a pulse source, which is presented by the electromotive force source E and the internal resistance $R1$, and at another end it is connected with the beginning of the meander line turn. The other two conductors are connected at the ends with resistors ($R2$ – $R5$) to ground. The meander microstrip line consists of two parallel conductors with the length l_{ML} interconnected at one end. One of the meander line conductors is connected to the end of the active conductor of the 3-conductor MF (at node $V5$). Another conductor of the line is connected to a receiving unit, which is shown as resistance $R6$. All resistances $R1$ – $R6$ are taken equal to 50Ω .

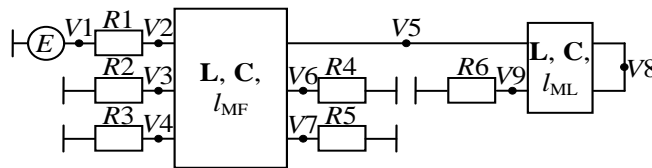


Figure 2. Schematic diagram of a cascade of a 3-conductor MF and a meander line.

As an excitation, we used a trapezoid pulse with emf of 1 V, flat top duration time of 100 ps, and rise and fall duration time of 50 ps each, similar to [16].

3. Preliminary analysis

It is known [14] that for certain parameters of the MF cross-section, the number of decomposition pulses at the end is equal to the number of MF conductors (2 pulses will be observed at the end of a 2-conductor MF, 3 pulses - of a 3-conductor MF, etc.), and when their number increases the amplitude of the signal at the end of the MF decreases. It is also known [15] that at the end of one turn of a meander line with optimal cross-section parameters, there will be 3 main decomposed pulses (crosstalk at the near end of the line and pulses of the odd and even line modes). Thus, with the optimal parameters of the cross-sections of the cascaded 3-conductor MF and the meander line, the output waveform will have 9 main decomposed pulses, because each of the 3 pulses from the end of the 3-conductor MF will decompose into 3 pulses in the meander line. However, to ensure this decomposition, it is necessary to formulate and fulfill the appropriate conditions.

As noted earlier, the number of modes propagating in multiconductor lines is equal to the number of conductors, with each mode having a specific per-unit-length delay [14]. Thus, in a 3-conductor MF, 3 modes propagate, each with its own per-unit-length delay (τ_1 , τ_2 , τ_3), and in a turn of a meander microstrip line, only odd (τ_o) and even (τ_e) modes propagate. It is important to note that in the meander line there is also near-end crosstalk, which arrives without delay. Then, knowing per-unit-length delays of each mode and lengths l_{MF} and l_{ML} , it is possible to determine the delays of each of the main decomposed pulses ($t_{P1}-t_{P9}$) at the end of the device under study, similar to [16]: $t_{P1}=\tau_1 l_{MF}$, $t_{P2}=\tau_1 l_{MF}+\tau_o 2 l_{ML}$, $t_{P3}=\tau_1 l_{MF}+\tau_e 2 l_{ML}$, $t_{P4}=\tau_2 l_{MF}$, $t_{P5}=\tau_2 l_{MF}+\tau_o 2 l_{ML}$, $t_{P6}=\tau_2 l_{MF}+\tau_e 2 l_{ML}$, $t_{P7}=\tau_3 l_{MF}$, $t_{P8}=\tau_3 l_{MF}+\tau_o 2 l_{ML}$, $t_{P9}=\tau_3 l_{MF}+\tau_e 2 l_{ML}$.

For the complete ultrashort pulse decomposition at the end of the device, it is necessary for the delay of each subsequent pulse to be more than the delay of the previous one summed with the total ultrashort pulse duration, otherwise the pulses will overlap. Knowing the expressions defining pulse delays ($P1-P9$), this can be ensured by the following series of conditions:

$$\tau_1 l_{MF}+\tau_o 2 l_{ML} \geq \tau_1 l_{MF}+t_{\Sigma}, \quad (1)$$

$$\tau_1 l_{MF}+\tau_e 2 l_{ML} \geq \tau_1 l_{MF}+\tau_o 2 l_{ML}+t_{\Sigma} \quad (2)$$

$$\tau_2 l_{MF} \geq \tau_1 l_{MF}+\tau_e 2 l_{ML}+t_{\Sigma}, \quad (3)$$

$$\tau_2 l_{MF}+\tau_o 2 l_{ML} \geq \tau_2 l_{MF}+t_{\Sigma}, \quad (4)$$

$$\tau_2 l_{MF}+\tau_e 2 l_{ML} \geq \tau_2 l_{MF}+\tau_o 2 l_{ML}+t_{\Sigma}, \quad (5)$$

$$\tau_3 l_{MF} \geq \tau_2 l_{MF}+\tau_e 2 l_{ML}+t_{\Sigma}, \quad (6)$$

$$\tau_3 l_{MF}+\tau_o 2 l_{ML} \geq \tau_3 l_{MF}+t_{\Sigma}, \quad (7)$$

$$\tau_3 l_{MF}+\tau_e 2 l_{ML} \geq \tau_3 l_{MF}+\tau_o 2 l_{ML}+t_{\Sigma}, \quad (8)$$

where t_{Σ} is the sum of the front, flat top and fall of the action.

After simple algebraic transformations, expressions (1), (4), (7) will take the following identical form:

$$\tau_o 2 l_{ML} \geq t_{\Sigma}, \quad (9)$$

and expressions (2), (5) and (8) will take the following identical form:

$$\tau_e 2l_{ML} \geq \tau_o 2l_{ML} + t_{\Sigma}. \quad (10)$$

Thus, in order to decompose an ultrashort pulse into a sequence of 9 pulses in a cascaded 3-conductor MF and a meander line, it is necessary to fulfill conditions (3), (6), (9) and (10).

4. Simulation results

Simulation was performed without losses in conductors and dielectric in the TALGAT software [15]. Taking into account conditions (3), (6), (9) and (10) a heuristic search was performed for optimal parameters of the MF and meander line cross-sections. The following MF cross-sectional parameters were obtained: $w_{MF}=500 \mu\text{m}$, $t_{MF}=200 \mu\text{m}$, $h_{MF}=1500 \mu\text{m}$, $s_{1MF}=10 \mu\text{m}$, $s_{2MF}=90 \mu\text{m}$ and $\epsilon_r_{MF}=25$. The meander line cross-section optimal parameters are the following: $w_{ML}=500 \mu\text{m}$, $t_{ML}=300 \mu\text{m}$, $h_{ML}=500 \mu\text{m}$, $s_{ML}=32 \mu\text{m}$ and $\epsilon_r_{ML}=80$.

The calculated **C** and **L** matrixes for MF are:

$$\mathbf{C} = \begin{bmatrix} 701.788 & -522.889 & -25.7018 \\ -522.889 & 833.382 & -209.232 \\ -25.7018 & -209.232 & 393.704 \end{bmatrix} \text{ pF/m}, \quad \mathbf{L} = \begin{bmatrix} 436.439 & 408.047 & 311.67 \\ 408.047 & 432.014 & 327.158 \\ 311.67 & 327.158 & 471.996 \end{bmatrix} \text{ nH/m}.$$

The calculated **C** and **L** matrixes for the meander line are:

$$\mathbf{C} = \begin{bmatrix} 1.79082 & -0.795507 \\ -0.795507 & 1.79082 \end{bmatrix} \text{ nF/m}, \quad \mathbf{L} = \begin{bmatrix} 278.427 & 229.597 \\ 229.597 & 278.427 \end{bmatrix} \text{ nF/m}.$$

Per-unit-length mode delays of the MF ($\tau_1=5.70 \text{ ns/m}$, $\tau_2=9.09 \text{ ns/m}$, $\tau_3=12.54 \text{ ns/m}$) and the meander line ($\tau_o=11.24 \text{ ns/m}$, $\tau_e=22.49 \text{ ns/m}$) were calculated from the **C** and **L** matrices [16]. Taking into account conditions (3), (6), (9) and (10), the MF and meander line lengths were obtained: $l_{MF}=1200 \text{ mm}$ and $l_{ML}=50 \text{ mm}$.

Based on the preliminary analysis results, the obtained per-unit-length mode delays and the lengths of the MF and meander microstrip line, we verify conditions (3), (6), (9) and (10). After substituting the known variables in (3), we obtain $10.92 \text{ ns} \geq 9.29 \text{ ns}$, in (6) – $15.04 \text{ ns} \geq 13.37 \text{ ns}$, in (9) – $1.12 \text{ ns} \geq 0.2 \text{ ns}$, and in (10) – $2.25 \text{ ns} \geq 1.32 \text{ ns}$. Thus, conditions (3), (6), (9) and (10) are fulfilled with a good margin.

Additionally, the delays of 9 main pulses were calculated (Table I). It can be seen that the delay of each pulse is more than that of the previous one by more than 0.2 ns.

Table 1. Calculated delays (ns) of each of the main pulses at the end of the device

t_{P1}	t_{P2}	t_{P3}	t_{P4}	t_{P5}	t_{P6}	t_{P7}	t_{P8}	t_{P9}
6.85	7.97	9.09	10.92	12.04	13.17	15.04	16.17	17.29

To confirm the foregoing, the time response of the device under investigation to the ultrashort pulse was calculated. Fig. 3 shows the output voltage waveform in the range of 6–18 ns (because after 18 ns only reflections with lower amplitude are observed) at the output under conditions (3), (6), (9) and (10). The output voltage is presented by a series of pulses with an amplitude less than 52 mV. The first pulse train ($S1$) is the result of the decomposition of the first mode pulse from the MF end into crosstalk and the odd and even modes in the meander line, the second ($S2$) – from the second mode pulse, and the third ($S3$) – from the third mode pulse. Thus, the pulses $P1$, $P4$, and $P7$ are crosstalk at the end of the meander line (node $V9$) from the pulses of the first (P_{m1}), second (P_{m2}), and third (P_{m3}) modes, respectively, coming from the MF to node $V5$. In this case, pulses $P2$ and $P3$ are pulses of an odd and even modes of the meander line from P_{m1} , $P5$ and $P6$ from P_{m2} , $P8$ and $P9$ from P_{m3} . It is also seen from Figure 3 that at the end of the device there are pulses of lower amplitude (in comparison with the main pulses) caused by reflections. As a result, the attenuation of the ultrashort pulse at the end of the device is 9.8 times (relative to half of the emf).

To provide additional verification of conditions (3), (6), (9) and (10), let us consider situations when they are not satisfied. First, we consider the situation when conditions (3) and (6) are not satisfied, for example, because of a decrease of l_{MF} to 700 mm and an increase of ultrashort pulse duration to 0.3 ns (due to the flat top). Figure 4 shows the output voltage waveform with $l_{MF}=700$ mm and $t_{\Sigma}=0.3$ ns. Here we also can see that pulse $P3$ overlaps pulse $P4$ and pulse $P6$ overlaps the pulse of the third sequence - $P7$. Moreover, Figure 4 shows that the pulses caused by reflections overlap pulses $P5$ and $P8$. In addition, the arrival time of all pulses decreased (in comparison with Figure 3). For example, the arrival time of pulse $P1$ decreased to 3.99 ns, and $P9$ – to 11.02 ns. The amplitude of the output voltage is 69 mV. After substituting the values of the variables in (3), we obtain 6.37 ns ≤ 6.44 ns, and in (6) – 8.77 ns ≤ 8.82 ns.

Let us consider the case when condition (9) is not fulfilled, for example, due to a decrease of s_{ML} and ϵ_{rML} , as well as l_{ML} . Figure 5 shows the waveform of the output voltage with $s_{ML}=10$ μ m, $l_{ML}=15$ mm, $\epsilon_{rML}=40$, $l_{MF}=1200$ mm and $t_{\Sigma}=0.2$ ns. Here we can see that the pulse rises of the odd modes $P2$, $P5$, and $P8$ overlap the falls of pulses $P1$, $P4$, and $P7$. The output voltage amplitude was 94 mV. After substituting the values of the variables in (9), we obtain 0.18 ns ≤ 0.2 ns.

Finally, we consider the case when condition (10) is not fulfilled. To do this, we reduce ϵ_{ML} to 10, and l_{ML} to 25 mm. Figure 6 shows the output voltage waveform of the output voltage at $\epsilon_{rML}=10$, $l_{ML}=25$ mm, $s_{ML}=32$ μ m, $l_{MF}=1200$ mm and $t_{\Sigma}=0.2$ ns. Here we can see that pulses P_{m1} , P_{m2} , and P_{m3} are not completely decomposed into pulses $P2$, $P5$, $P8$ and $P3$, $P6$, $P9$. In this case, the signal amplitude at the end of the line was 72 mV. After substituting the values of the variables in (10), we obtain 0.41 ns ≤ 0.45 ns.

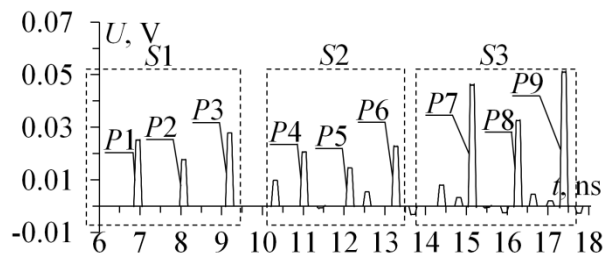


Figure 3. Output voltage waveform under conditions (3), (6), (9) and (10).

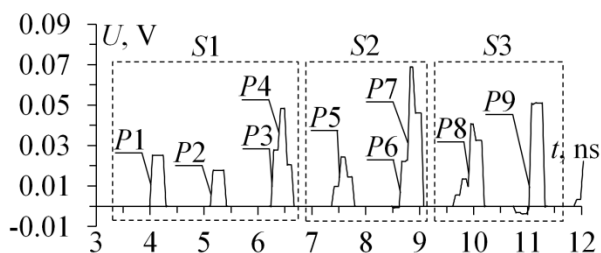


Figure 4. Output voltage waveform with $l_{MF}=700$ mm and $t_{\Sigma}=0.3$ ns.

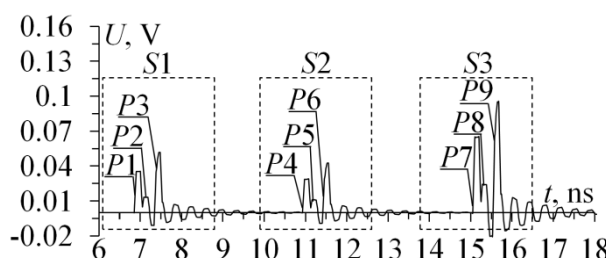


Figure 5. Output voltage waveform with $s_{ML}=10$ μ m, $l_{ML}=15$ mm, $\epsilon_{rML}=40$, $l_{MF}=1200$ mm and $t_{\Sigma}=0.2$ ns.

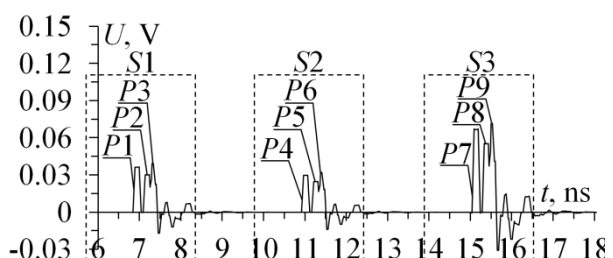


Figure 6. Output voltage with $\epsilon_{rML}=10$, $l_{ML}=25$ mm, $s_{ML}=32$ μ m, $l_{MF}=1200$ mm and $t_{\Sigma}=0.2$ ns.

5. Conclusion

The study has demonstrated the feasibility of ultrashort pulse decomposition in a hybrid device consisting of a 3-conductor MF and a meander microstrip line and formulated a number of conditions which provide such decomposition. As a result, we obtained the attenuation of an ultrashort pulse of 9.8 times (relative to the input signal).

It should be noted that the obtained optimal parameters, which provide the necessary conditions, are difficult to implement in practice (for example, due to the large values of s_{1MF} and ϵ_{rML}), and the MF

length ($l_{MF}=1200$ mm) is large, for example, for use in the spacecraft onboard EE. In addition, for practical application of such device, it is necessary to take into account its matching with the tract of 50Ω (mainly in radio engineering), which has not been discussed in this paper. However, it is possible to satisfy the necessary conditions by choosing other values of cross-section parameters (implementable in practice), which also ensure the matching of the line with the tract. This could be achieved through global optimization by genetic algorithms which make it possible to find optimal parameters, setting their range, and also use one or more optimization criteria.

Thus, the presented results allow us to state that, if the appropriate conditions are fulfilled in the device for protection against ultrashort pulses consisting of a 3-conductor MF and a meander microstrip line, it is possible to minimize the amplitude of the ultrashort pulse. Minimization is achieved through ultrashort pulse decomposition into mode pulses in a 3-conductor MF, and then each of them into a crosstalk and pulses of the odd and even modes in the meander line turn.

6. Acknowledgments

The study was supported by state contract 8.9562.2017/8.9 of the Ministry of Education and Science of the Russian Federation and the Russian Foundation for Basic Research grant 18-37-00339\18.

References

- [1] Meshcheryakov S A 2013 *Journal of Radio Electronics* **12** 1–15
- [2] Pirogov Y A and Solodov A V 2013 *Journal of radio electronics* **6** 1–38
- [3] Gizatullin Z M and Gizatullin R M 2016 *Journal of Communications Technology and Electronics* **61(5)** 546–50
- [4] Mora N, Vega F, Lugin G, Rachidi F and Rubinstein M 2014 Study and classification of potential IEMI sources *System and assessment notes* **Note 41** pp 1–48
- [5] Gizatullin Z M and Gizatullin R M 2014 *Journal of Communications Technology and Electronics* **59(5)** 424–26
- [6] Messier M A, Smith K S, Radasky W A and Madrid M J 2003 Response of telecom protection to three IEC waveforms *Proc. of the 15th Int. Zurich Symp. on EMC (Zurich)* pp 127–132
- [7] Krzikalla R, Luikenter J, ter Haseborg L and Sabath F 2007 Systematic description of the protection capability of protection elements *Proc. of IEEE Int. Symp. on EMC (Honolulu)* pp 1–4
- [8] Krzikalla R, Weber T and Haseborg J L 2003 *Proc. of IEEE Int. Symp. on EMC (Istanbul)* pp 1313–16
- [9] Krzikalla R and Haseborg J L 2005 *Proc. of IEEE Int. Symp. on EMC (Chicago)* pp 977–81
- [10] Weber T, Krzikalla R and Haseborg J L 2004 *IEEE Trans. on EMC* **46(3)** 423–30
- [11] Cui Q, Dong S and Han Y 2012 Investigation of waffle structure SCR for electrostatic discharge (ESD) protection *IEEE Int. Conf. on Electron Devices and Solid State Circuit (Bangkok)* pp 1–4
- [12] Hayashi H, Kuroda T, Kato K, Fukuda K, Baba S and Fukuda Y 2005 *Int. Conf. on Simulation of Semiconductor Processes and Devices (Tokyo)* pp 99–102
- [13] Belousov A O and Gazizov T R 2018 *Complexity* **2018** 15
- [14] Nosov A V, Surovtsev R S and Gazizov T R 2018 Ultrashort pulse decomposition in meander microstrip line of two turns *2018 Siberian Symposium on Data Science and Engineering (Novosibirsk)* pp 79–83
- [15] Kuksenko S P 2019 *IOP Conf. Series: Materials Science and Engineering* **560** 1–7
- [16] Malyutin N D 1990 Multi-connected stripe-geometry structures and devices based on them (Tomsk: Tomsk State University) p 164